Progress In Electromagnetics Research C, Vol. 77, 49–56, 2017

A Compact Wide Bandpass Filter with Good Selectively

Mengkui Shen[1, 2, *], Xianqi Lin[1], Jing Ai[1, 2], Cong Tang[1], and William T. Joines[2]

Abstract—A compact Ku-band bandpass filter (BPF) with wide passband, compact size and high selectively is presented. The presented BPF is composed of two quarter-wavelength resonators and a dual-mode resonator, resulting in a compact circuit size. The transmission zeros (TZs) located at the lower and upper stopband are achieved by the mixed electromagnetic (EM) coupling and dual-mode resonator, respectively, resulting in a high frequency selectively. The measured results show minimum in-band insertion loss, fractional bandwidth and variation of group delay to be 0.9 dB, 36.2% and 0.12 ns, respectively. Also, the stopband suppression is greater than 28 dB from 5 to 10.3 GHz and 30 dB from 19.5 to 29.5 GHz. The effective circuit size of the filter is $8.43 \times 2.28\,\text{mm}^2$ ($0.63\lambda_g \times 0.17\lambda_g$, where λ_g is the guide wavelength of 15.1 GHz).

1. INTRODUCTION

With the rapidly development of wideband wireless communication, microwave wideband filters, as one of the most important passive components in high-speed wireless communication systems, are used to reduce the signal crosstalk between adjacent channels and for the suppression of clutter in the highly selective stopbands.

In recent work, structure loaded resonators (SLRs) and stepped impedance resonators (SIRs) in microstrip have been used extensively in wideband filters [1–4]. This is true because the resonators have desirable multimode resonance characteristics, realized by exciting different resonant modes in a composite resonator, and the mixed EM coupling induces TZs in the stopband through separate electric and magnetic coupling paths [5–8]. Compared to cross-coupling and source-load coupling, mixed EM coupling structures are simpler, and the induced TZs are controllable, thus they are now being studied extensively. In [9–11], a dual-mode resonator and mixed electric and magnetic coupling structure are used together to design filters with small size and good selectivity, but their operation passbands are in the radio frequency. In addition, the composite right/left-handed transmission lines are also used to design wideband or harmonic suppressed devices [12–15], but the circuits are complicated, and most of them have large size.

In this work, a compact Ku-band BPF is described, and it combines hybrid resonator and mixed EM coupling to improve frequency selectivity. The mixed EM coupling with separate coupling paths is used between the quarter-wavelength resonator and dual-mode resonator, in which a coupling gap and a high-impedance transmission line are used to realize the electric and magnetic couplings, respectively. The dual-mode resonator achieves a TZ at the upper stopband, and the mixed EM coupling introduces two TZs at the lower stopband. The results show that this filter exhibits exceptional good frequency selectivity due to the generation of TZs in the stopband. Also, the filter has compact size, wideband, low insertion loss and linear response.

Received 31 May 2017, Accepted 9 August 2017, Scheduled 21 August 2017

* Corresponding author: Mengkui Shen (mkshen01@163.com).

[1] EHF Key Laboratory of Fundamental Science, University of Electronic Science and Technology of China, Chengdu 611731, P. R. China. [2] Department of Electrical and Computer Engineering, Duke University, Durham, USA.

2. FILTER DESIGN

2.1. Resonator Analysis

Figure 1 shows the configuration of proposed BPF, which consists of hybrid resonator and mixed EM coupling. Fig. 2 shows the dual-mode resonator, it mainly consists of a half-wavelength resonator and a stepped impedance stub. Fig. 2(a) shows the basic structure of the dual-mode resonator, where L_1 and Y_1 are the length and characteristic admittance of the half-wavelength transmission line; L_2 and Y_2 are the length and characteristic admittance of the high impedance sections of the stepped impedance stub; L_3 and Y_3 are the length and characteristic admittance of the low impedance sections of the stepped impedance stub. Obviously, the dual-mode resonator is symmetric, so it can be characterized by odd- and even-mode theory, and the equivalent circuit mode is shown in Fig. 2(b). The final dimensions of the parameters are given by 3D electromagnetic simulator, and the dimensions in Fig. 1 are: $l1 = 7.58$, $w1 = 0.22$, $l2 = 0.78$, $w2 = 0.72$, $le = 2.53$, $l3 = 2.32$, $w3 = 1.11$, $l4 = 2.58$, $w4 = 0.12$, $l5 = 1.68$, $w5 = 0.1$, $lm = 2.58$, $wm = 0.1$, $s1 = 0.19$, $s2 = 0.1$ mm, $dm = 0.3$, $D1 = 0.15$, $D2 = 0.25$ (unit: mm).

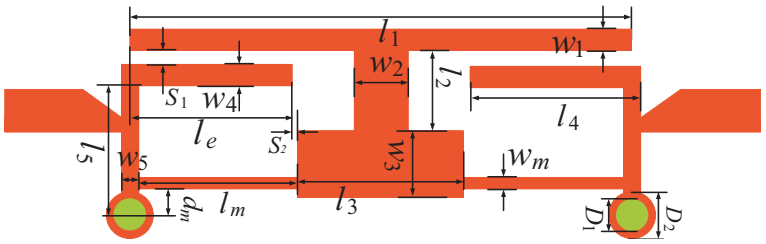

Figure 1. Configuration of the proposed wideband filter.

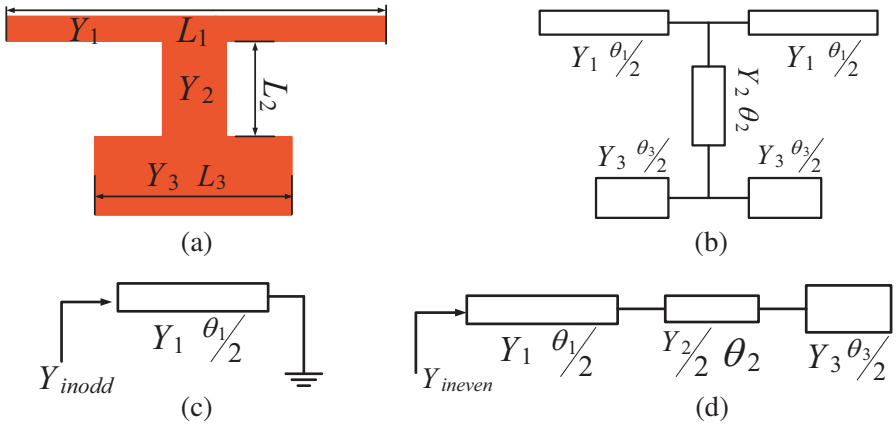

Figure 2. Dual-mode resonator. (a) Structure. (b) Equivalent circuit. (c) Odd-mode equivalent circuit. (d) Even-mode equivalent circuit.

When the dual-mode resonator is excited by odd-mode, the voltage in symmetrical plane is zero, so the symmetrical plane can be seen as ideal electric wall and equivalent to virtual short-circuited end. Therefore, the odd-mode equivalent circuit can be given as in Fig. 2(c), and the input admittance $Y_{in_{odd}}$ is calculated as

$$Y_{i_{odd}} = \frac{Y_1}{j\tan(\theta_1/2)} \tag{1}$$

where $\theta_1 = \beta L_1$ is the electrical length of the half-wavelength microstrip line. According to the resonance condition of $\mathrm{Im}\{Y_{in_{odd}} = 0\}$, the odd-mode resonance frequency f_o can be obtained as

$$f_o = \frac{(2n-1)c}{2L_1\sqrt{\varepsilon_{eff}}} \quad n = 1, 2, 3\ldots \tag{2}$$

where c is the propagation velocity of light in vacuum, and ε_{eff} is the effective dielectric constant. From Equation (2), we know that the stepped impedance stub has no influence on the odd-mode resonance frequency, which is only related with the length of the half-wavelength microstrip line.

When the dual-mode resonator is excited by even-mode, there is no current in the symmetry plane, thus the symmetry plane can be seen as ideal magnetic wall and equivalent to virtual open-circuited end. The even-mode equivalent circuit is shown in Fig. 2(d). To simplify the analysis, $Y_1 = Y_2/2$ is assumed, so the input admittance $Y_{in_{even}}$ can be calculated as

$$Y_{in_{even}} = Y_1 \frac{jY_1 \tan\left(\frac{\theta_1}{2} + \theta_2\right) + jY_3 \tan\frac{\theta_3}{2}}{Y_1 - Y_3 \tan\frac{\theta_3}{2} \tan\left(\frac{\theta_1}{2} + \theta_2\right)} \tag{3}$$

where $\theta_2 = \beta L_2$, $\theta_3 = \beta L_3$ are the electrical length of the high and low impedance sections of the stepped impedance stub. By enforcing $\mathrm{Im}\{Y_{in_{even}} = 0\}$, the even-mode resonance frequency can be derived as

$$Y_3 \tan\frac{\theta_3}{2} + Y_1 \tan\left(\frac{\theta_1}{2} + \theta_2\right) = 0 \tag{4}$$

$$Y_3 \tan\left(\frac{\pi f_e}{c} L_3\right) + Y_1 \tan\left(\frac{\pi f_e}{c} L_1 + \frac{2\pi f_e}{c} L_2\right) = 0 \tag{5}$$

From Equation (5) we know that when the substrate and the ratio of Y_2/Y_1 are given, the even-mode resonance frequency is not only decided by the length of the half-wavelength microstrip line ($L1/2+L2$), but also decided by the length of stepped impedance stub $L3$. When the lengths of $L1$ and $L2$ are decided, f_e is only decided by $L3$, the longer the $L3$, the lower the f_e.

Figure 3 shows how the transmission poles (TPs) vary with different parameters. It is known that f_{p2} and f_{p3} decrease as $L5$ increases, because the longer the quarter-wavelength is, the lower the resonance frequency is. Further, the f_{p4} decreases as $L3$ increases, and f_{p1} has no change as $L3$ increases. According to the analysis of Equations (1)–(5), f_{p1} and f_{p4} are odd-mode and even-mode resonant frequency, respectively. Thus, from the above analysis, there are four TPs in the passband. f_{p1} and f_{p4} are introduced by the dual-mode resonator, while f_{p2} and f_{p3} are introduced by the two quarter-wavelength resonators.

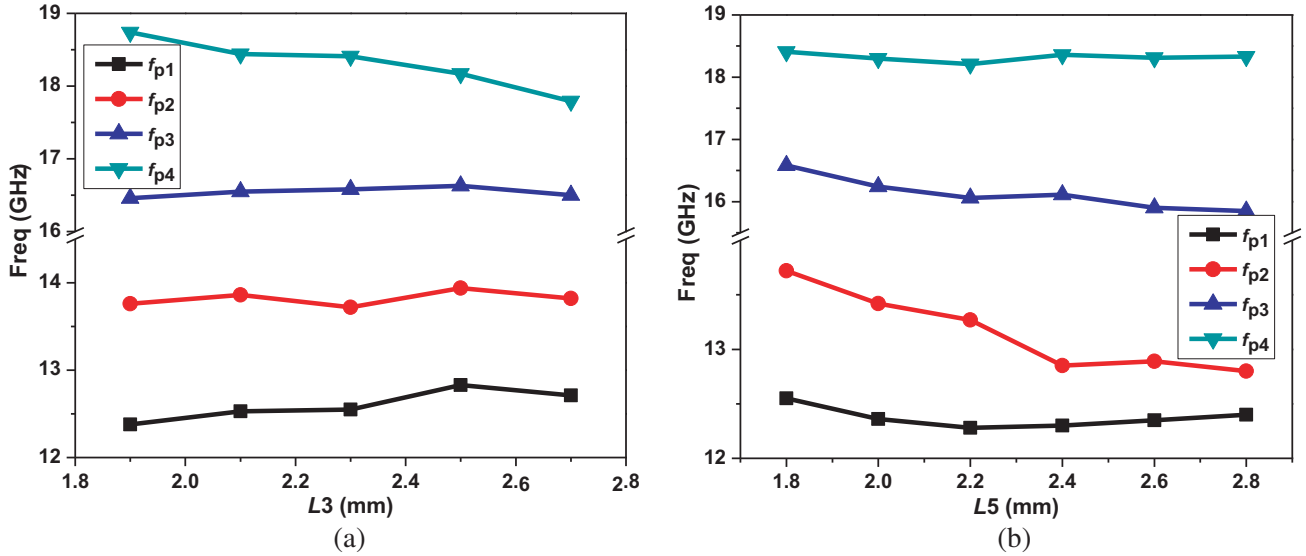

Figure 3. Transmission poles varied with different parameters. (a) $L3$ varied. (b) $L5$ varied.

2.2. Transmission Zeros Analysis

According to admittance function of the odd- and even-modes, the transfer function of the dual-mode structure can be given as

$$S_{21} = \frac{Y_0(Y_{in_{odd}} - Y_{in_{even}})}{(Y_0 + Y_{in_{odd}})(Y_0 + Y_{in_{even}})} \tag{6}$$

By setting $S21 = 0$, the transmission zero introduced by the dual-mode structure can be calculated as

$$Y_3 \tan\theta_2 \tan\frac{\theta_3}{2} = Y_1 \tag{7}$$

$$Y_3 \tan\left(\frac{2\pi L_2}{c} f_m\right) \tan\left(\frac{\pi L_3}{c} f_m\right) = Y_1 \tag{8}$$

It can be seen from Equation (8) that when L_2 is decided, TZ f_m is decided by the length of stepped impedance stub L_3, the more the length, the lower the transmission zero.

Figure 4 shows the variation of TZs versus different parameters. As shown in Fig. 4(a), the TZ in upper stopband range moves to the left when the values of $L3$ increase, which confirms the result in Equation (8). Fig. 4(b) shows that TZs in down stopband range shifts to right as *dm* increases, as a result of the Mc increases with *dm*.

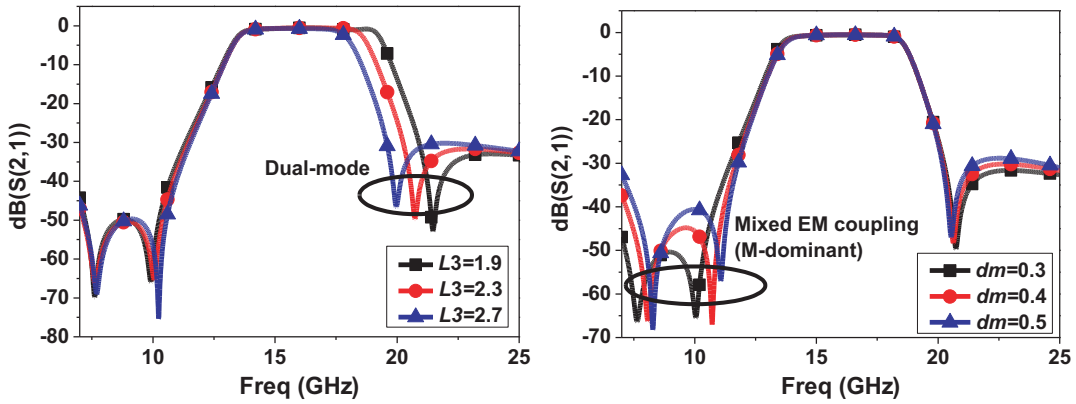

Figure 4. Simulated $S21$ with different value. (a) Simulated $S21$ with varied $L3$. (b) Simulated $S21$ with varied *dm*.

The topology of the mixed coupling structure in the fourth-order filter is shown in Fig. 5. It shows that there are two separate coupling paths between resonators 1 and 2, as well as resonators 3 and 4. One of the coupling paths is electrical coupling, which is realized by the gap ($s1$) of the parallel coupling lines. Another coupling path is magnetic coupling, which is realized by a high-impedance line that connects the two resonators (1 and 2 or 3 and 4) and acts as a coupling inductance.

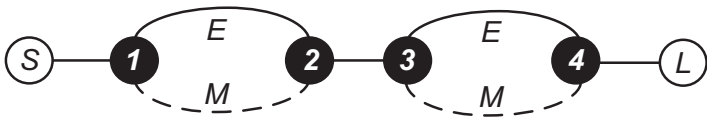

Figure 5. Topology diagram of proposed wideband filter.

From [16], the TZs induced by mixed electric and magnetic couplings can be controlled by choosing different electrical and magnetic couplings. TZ is located at the lower frequency when the magnetic coupling is dominant and located at the higher frequency when the electric coupling is dominant. Thus, by increasing the magnetic coupling between resonators 1 and 2, a TZ is induced in the lower stopband.

Meanwhile, it also induces a TZ in the lower stopband when the magnetic coupling between resonators 3 and 4 is dominant. Fig. 3(b) shows that the TZs in the lower stopband shift to the left with decreasing dm, i.e., the TZs induced by mixed electric and magnetic couplings move to the lower frequency with increasing magnetic coupling.

Figure 6 shows the frequency responses of proposed structure with and without the high-impedance lines. It can be seen that when the high-impedance lines are added, two TZs (TZ1 and TZ2) are introduced. This is because the high-impedance lines introducing magnetic coupling paths between resonators 1 and 2 and resonators 3 and 4, respectively, as shown in Fig. 4. The magnetic coupling combined with electric coupling leads to TZ1 and TZ2. TZ3 is introduced by the dual-mode resonator, as the analysis of Equations (6)–(8).

It is known that the coupling between resonators 1 and 2, as well as between resonators 3 and 4, is mixed EM coupling. The magnetic coupling Mc is realized by the high-impedance lines, and the electric coupling Ec is realized by the gap of the parallel coupled lines. The mixed coupling coefficient $k = (Mc - Ec)/(1 - McEc)$. The TZ1 and TZ2 are located at the lower stopband because the Ec is stronger than Mc. The TZs introduced by mixed EM coupling is determined by $f_m = f_r\sqrt{M_C/E_C}$.

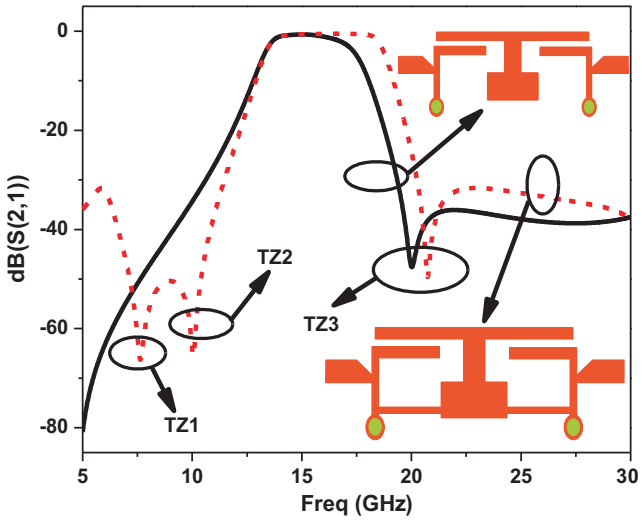

Figure 6. Frequency responses of proposed structure with and without high-impedance lines.

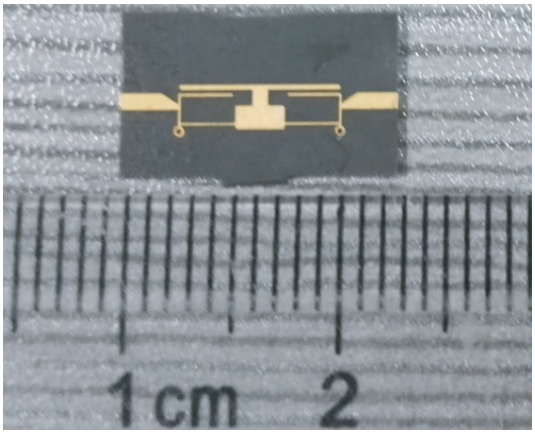

Figure 7. Photograph of the fabricated filter.

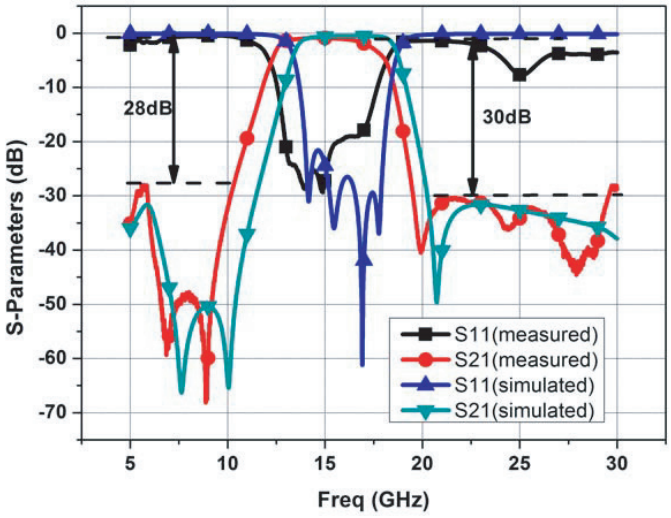

Figure 8. Simulated and measured S-parameters.

3. EXPERIMENTAL RESULTS

The proposed filter is designed and fabricated on a Rogers RT/duroid 5880 substrate with a thickness of 0.254 mm, and its relative dielectric constant and loss tangent are 2.2 and 0.0009, respectively. Fig. 7 shows a photograph of the fabricated BPF, which has an effective size of $0.63 \times 0.17\lambda_g$ (λ_g is the guide wavelength at the central frequency).

Figure 8 shows the measured S-parameters, and the simulated results are also given for comparison. The measured 3 dB bandwidth is 5.47 GHz (FBW = 36.2%), and the measured insertion losses at central frequency is 0.9 dB. The return loss is better than 15 dB. The measured rejection from DC to 10.3 GHz is greater than 28 dB due to the two transmission zeros located at 6.8 GHz and 8.9 GHz, and the rejection from 19.5 GHz to 29.5 GHz is greater than 30 dB due to the transmission zero located at 19.9 GHz. The simulated and measured group delays are shown in Fig. 9(a). The figure shows that the measured group delay is varied from 0.32 ns to 0.44 ns over the whole passband range, which is small enough for high linearity system applications. As shown in Fig. 8 and Fig. 9(a), the measured results shift to the low

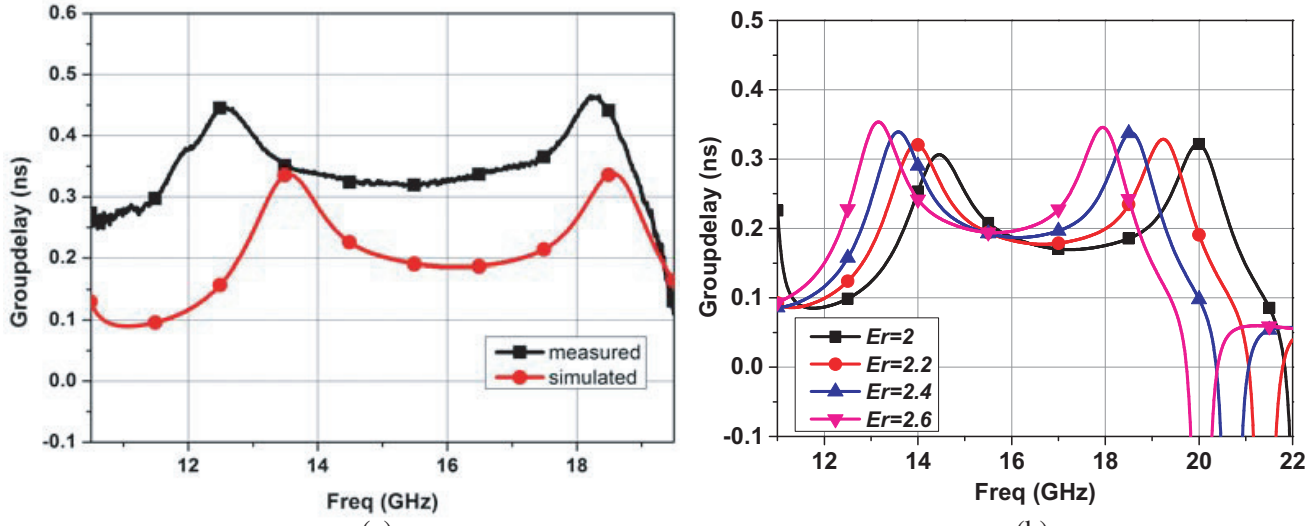

Figure 9. Groupdelay. (a) Simulated and measured results. (b) Simulated results with varied Er.

Table 1. Comparison with other similar bandpass filters.

REF.	Center frequency (GHz)	FBW	IL (dB)	Group delay Variation (ns)	Size (λ_g^2)	Stopband with Rejection > 28 dB (GHz)	
						upper	lower
[17]	25.5	20%	> 2	< 0.184	1.25 × 1.12	37.5–40	DC-11
[18]	14.5	24%	> 0.46	-	0.63 × 0.33	19–27	DC-11
[19]	4.13	7.26%	> 1.78	-	0.4 × 0.53	4.6–5	DC-3.8
[20]	11.94	10.8%	> 1.7	-	0.63 × 0.19	13.2–13.5	10-10.7
[21]	8.68	12.9%	> 1.43	< 0.7	1.35 × 0.4	10–14	DC-8
[22]	5.15	45%	> 1.2	< 0.2	0.98 × 0.37	7.5–12.5	DC-2
This work	15.1	36.2%	> 0.9	< 0.12	0.63 × 0.17	19.5–30	DC-10.5

λ_g is the guided wavelength of 50 Ohm microstrip at the center frequency of each filter.

frequency compared with the simulated ones. It is mainly caused by the inevitable error in fabrication and variation of relative dielectric constant. Fig. 9(b) shows that the group delay changes as the relative dielectric constant is varied, which also moves the resonance frequencies.

In the process of fabricating high frequency PCBs, the substrates are easily deformed because they are thin and soft, which changes the size of resonator and coupling structure, and consequently, the resonance frequencies and bandwidth are changed. In addition, the dielectric constant of Rogers RT/duroid 5880 is 2.2 at 10 GHz, but it is changed when working at 15 GHz, which also affects the strength of coupling and resonance frequencies.

The comparison with some reported similar BPFs is presented in Table 1 [13–18]. It shows that the proposed filter achieves wider bandwidth except the design in [18], lower insertion loss except the design in [14], lower group delay variation in the passband range, smaller size and better frequency selectivity.

4. CONCLUSIONS

A novel Ku-band BPF using mixed electric and magnetic couplings and hybrid resonator is designed, fabricated and tested. A dual-mode resonator and quarter-wavelength resonator are used in the design, resulting in a compact size. The mixed electric and magnetic coupling is used between the dual-mode resonator and quarter-wavelength resonator, resulting in two transmission zeros located in the lower stopband. In addition, the dual-mode also induces a transmission zero in the upper stopband. The proposed filter has the advantages: wide bandwidth, compact size, easy fabrication, good selectivity and low insertion loss, all of which are desirable for high-speed wireless communication and high-precision imaging applications.

ACKNOWLEDGMENT

This work was supported in part by NSFC (Nos. 61571084 and 61561021), in part by NCET (No. NCET-13-0095), in part by the FRF for CU (No. ZYGX2014J016), and in part by the SRF for ROCS, SEM.

REFERENCES

1. Li, R. and L. Zhu, "Compact UWB bandpass filter using stub-loaded multiple-mode resonator," *IEEE Microw. Wireless Compon. Lett.*, Vol. 17, No. 1, 40–42, Jan. 2007.
2. Chen, C. F., C. Y. Lin, J. H. Weng, and K. L. Tsai, "Compact microstrip broadband filter using multimode stub-loaded resonator," *Electron. Lett.*, Vol. 49, No. 8, 545–546, 2013.
3. Ouyang, Z. A. and Q. X. Chu, "An improved wideband balanced filter using internal cross-coupling and $3/4\lambda$ stepped-impedance resonator," *IEEE Microw. Wirel. Compon. Lett.*, Vol. 26, No. 3, 156–158, 2016.
4. Shen, M. K., Z. H. Shao, C. J. You, and F. S. Ban, "Ku-band compact bandpass filter with wide upper stopband using multilayer LCP technology," *Microw. Optical Tech. Lett.*, Vol. 57, No. 5, 1121–1125, 2015.
5. Xiao, J. K., M. Zhu, Y. Li, and J. G. Ma, "Coplanar waveguide bandpass filters with separated electric and magnetic couplings," *Electron. Lett.*, Vol. 52, No. 2, 122–124, 2016.
6. Wang, H. and Q. X. Chu, "An inline coaxial quasi-elliptic filter with controllable mixed electric and magnetic coupling," *IEEE Trans. Microw. Theory Tech.*, Vol. 57, No. 3, 667–673, 2009.
7. Xiao, J.-K., M. Zhu, Y. Li, T. Li, and J.-G. Ma, "High selective microstrip bandpass filter and diplexer with mixed electromagnetic coupling," *IEEE Microw. Wirel. Compon. Lett.*, Vol. 25, No. 12, 781–783, 2015.
8. Yuan, S. L., X. B. Wei, G. T. Yue, and M. X. Zhang, "Cascaded fourth-order mixed-coupled bandpass filter with good frequency selectivity," *International Workshop on Microwave and Millimeter Wave Circuits and System Technology*, 229–232, 2013.
9. Xu, J., "Compact tunable wideband bandpass filter using mixed coupling lumped dual-mode resonator," *Journal of Electromagnetic Waves and Applications*, Vol. 30, No. 6, 714–720, 2016.

10. Xu, J., "Compact quasi-elliptic response wideband bandpass filter with four transmission zeros," *IEEE Microw. Wirel. Compon. Lett.*, Vol. 25, No. 3, 169–171, 2015.
11. Tang, S. C., J. T. Kuo, and S. J. Chung, "Bandwidth and transmission zero control for compact dual-mode resonator filter by extraction of EM coupling," *Asia Pacific Microwave Conference Proceedings (APMC)*, 661–663, 2012.
12. Xu, H. X., G. M. Wang, and C. X. Zhang, "Fractal-shaped UWB bandpass filter based on composite right/left handed transmission line," *Electron. Lett.*, Vol. 46, No. 4, 285–286, 2010.
13. Xu, H. X., G. M. Wang, Z. M. Xu, X. Chen, Z. W. Yu, and L. Geng, "Dual-shunt branch circuit and harmonic suppressed device application," *Applied Physics A*, Vol. 108, No. 2, 497–502, 2012.
14. Xu, H. X., G. M. Wang, and J. G. Liang, "Novel composite right/left handed transmission lines using fractal geometry and compact microwave devices application," *Radio Sci.*, Vol. 46, RS5008, 2011.
15. Xu, H. X., G. M. Wang, C. X. Zhang, and X. Wang, "Characterization of composite right/left handed transmission line," *Electron. Lett.*, Vol. 47, No. 18, 1030–1032, 2011.
16. Chu, Q. X. and H. Wang, "A compact open-loop filter with mixed electric and magnetic coupling," *IEEE Trans. Microw. Theory Tech.*, Vol. 56, No. 2, 431–439, 2008.
17. Cai, P., Z. W. Ma, X. H. Guan, G. X. Zheng, A. Tetsuo, and H. Gen, "A compact and low-loss sub-millimeter-wave ultra-wideband bandpass filter," *Microw. Optical Tech. Lett.*, Vol. 49, No. 2, 481–484, 2007.
18. Zhu, W. S., J. R. Zhang, and M. X. Yu, "A novel Ku-band microstrip triple-mode filter using stub-loaded resonator," *International Conf. Electronics, Communications and Control (ICECC)*, 1847–1849, 2011.
19. Avinash, K. G. and I. S. Rao, "Compact dual-mode microstrip bandpass filters with transmission zeros using modified star shaped resonator," *Progress In Electromagnetics Research C*, Vol. 71, 177–187, 2017.
20. Maharjan, R. K., B. Shrestha, and N. Y. Kim, "Compact microstrip square open-loop bandpass filter using open stub," *Electron. Lett.*, Vol. 48, No. 6, 333–334, 2012.
21. Ge, C., X. W. Zhu, W. C. Zhu, and X. Jiang, "Synthesis design of box-section bandpass filter with hybrid and dual-mode resonators," *IEEE Microw. Wirel. Compon. Lett.*, Vol. 24, No. 12, 836–838, 2014.
22. Ma, K., K. C. B. Liang, R. M. Jayasuriya, and K. S. Yeo, "A wideband and high rejection multimode bandpass filter using stub perturbation," *IEEE Microw. Wirel. Compon. Lett.*, Vol. 19, No. 1, 24–26, 2009.